

Topological Analysis of the Charge Density in Short Intramolecular O—H···O Hydrogen Bonds. Very Low Temperature X-ray and Neutron Diffraction Study of Benzoylacetone

Georg Kent Hellerup Madsen,[†] Bo Brummerstedt Iversen,[†] Finn Krebs Larsen,^{*,†} Moshe Kapon,[‡] George M. Reisner,[‡] and Frank H. Herbstein[‡]

Contribution from the Departments of Chemistry, University of Aarhus, DK-8000 Århus C, Denmark, and Technion, Israel Institute of Technology, Haifa, Israel 32000

Received January 20, 1998. Revised Manuscript Received August 5, 1998

Abstract: A study of intramolecular hydrogen bonding in benzoylacetone (1-phenyl-1,3-butadiene) has been carried out with 8.4(4)K X-ray data and 20(1)K neutron data. Analysis of the neutron data shows that the hydrogen, between the two oxygens in the keto–enol part of the molecular structure, is asymmetrically placed in a large flat potential well. The charge density obtained from X-ray and neutron data has been analyzed by using multipolar functions and topological methods, which gave evidence of extensive π -delocalization in the keto–enol group. The multipole populations show that there are large formal charges on the oxygens and the enol hydrogen, which impart polar character to the hydrogen bond. This effect is also evident in the Laplacian and in the electrostatic potential calculated from the X-ray data and it is found that the hydrogen position is stabilized by both electrostatic and covalent bonding contributions at each side of the hydrogen atom. The resonance assisted hydrogen bonding model has been refined to reflect the redistribution of charge.

Introduction

In recent years much attention has been directed toward trying to understand the nature of the bonding in low-barrier short hydrogen bonds and their role in enzyme catalysis.¹ Gilli, Bellucci, Ferretti, and Bertolasi² have proposed the resonance assisted hydrogen bonding (RAHB) model to account for the very short O—H···O and N—H···O distances observed in conjugated neutral systems containing hydrogen bonds. Many examples of such conjugated systems have been found among the β -diketone enols, where O—H···O distances ranging from 2.37³ to about 2.7 Å could be related to the π delocalization of the O=C—C=C—O—H keto–enol group. The essence of the RAHB model for a *cis*-enol fragment is illustrated by scheme a shown in Figure 1. As originally proposed by Gilli et al.² the π -electron delocalization introduces partial charges at the oxygens. Consequently, the energy of the system is lowered

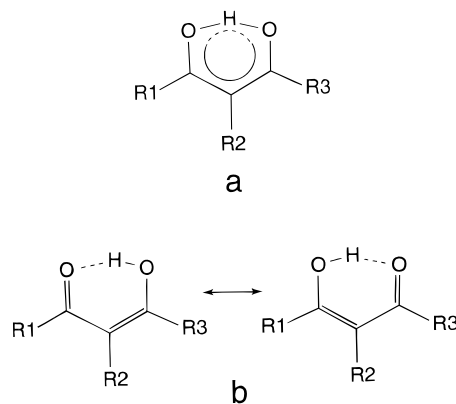


Figure 1. Models for short hydrogen bonds: (a) the resonance assisted hydrogen bonding model; (b) the two tautomers of the disordered model.

as the positive hydrogen nucleus moves toward the negative keto oxygen atom. Thus, Gilli's RAHB model can be conceived as a feedback mechanism, which maintains zero partial charge on the two opposite oxygens by neutralizing the increase in polarization due to resonance with a decrease caused by a shift in the proton position in the hydrogen bond.⁴ The strengthening of the O—H···O bond, as indicated by the shortening of d_{O-O} , coincides with a lengthening of d_{O-H} . The RAHB *cis*-enol system is characterized by a large degree of charge delocalization and symmetry of the keto–enol group.

Scheme b in Figure 1 illustrates an alternative explanation for the observation that bond lengths in *cis*-enol systems are intermediate between single and double bonds. If the molecules have statistically disordered keto–enol systems, the hydrogen atoms of the hydrogen bond will be distributed over two

* To whom correspondence should be addressed. email: kre@kemi.aau.dk.

[†] University of Aarhus.

[‡] Israel Institute of Technology.

(1) (a) Cleland, W. W.; Kreevoy M. M. *Science* **1994**, *264*, 1887–1890. (b) Frey, P. A.; Whitt, S. A.; Tobin, J. B. *Science* **1994**, *264*, 1927–1930. (c) Tobin, J. B.; Whitt, S. A.; Cassidy, C. S.; Frey, P. A. *Biochemistry* **1995**, *34*, 6919–6924. (d) Garcia-Viloca, M.; Gonzalez-Lafont, A.; Lluch, J. M. *J. Am. Chem. Soc.* **1997**, *119*, 1081–1086. (e) McAllister, M. A. *Can. Chem.* **1997**, *75*, 1195–1202. (f) Pan, Y.; McAllister, M. A. *J. Am. Chem. Soc.* **1997**, *119*, 7561–7566. (g) Pan, Y.; McAllister, M. A. *J. Am. Chem. Soc.* **1998**, *120*, 166–169. (h) Smallwood, C. J.; McAllister, M. A. *J. Am. Chem. Soc.* **1997**, *119*, 11277–11281. (i) Pan, Y.; McAllister, M. A. *J. Org. Chem.* **1997**, *62*, 8171–8176. (j) Platts, J. A.; Laidig, K. E. *J. Phys. Chem.* **1996**, *100*, 13455–13461. (k) Tuckerman, M. E.; Marx, D.; Klein, M. L.; Parrinello, M. *Science* **1997**, *275*, 817–820. (l) Warshel, A.; Papazyan, A.; Kollman, P. A. *Science* **1995**, *269*, 102–104.

(2) (a) Gilli, G.; Bellucci, F.; Ferretti, V.; Bertolasi, V. *J. Am. Chem. Soc.* **1989**, *111*, 1023–1028. (b) Gilli, P.; Ferretti, V.; Bertolasi, V.; Gilli, G. *Advances in Molecular Structure Research*; Hargittai, M., Hargittai, I., Eds.; JAI Press: Greenwich, CT, 1996; Vol. 2, pp 67–102.

(3) Power, L. F.; Jones, R. D. G.; Pletcher, J.; Sax, M. *J. Chem. Soc.* **1975**, 1818–1821.

(4) Bertolasi, V.; Gilli, P.; Ferretti, V.; Gilli, G. *J. Am. Chem. Soc.* **1991**, *113*, 4917–4925.

positions in the crystal structure. Indeed this was the case for the C polymorph of naphthazarin above 110 K; at this temperature there is a second-order transition to a state with ordered enol hydrogen.⁵

Especially for room temperature diffraction studies the observed atomic displacement of the hydrogen atom around its average position is usually so substantial that it is impossible to judge whether the hydrogen atom is distributed over two positions (statistically or residing in a double minimum) or is moving in a shallow potential well. If the thermal energy of the hydrogen atom is sufficiently high, it is conceivable that a double minimum potential may be disguised as dynamic disorder. Thus it is clearly desirable to carry out diffraction studies of hydrogen bonding at the lowest possible temperatures.⁶

Very short hydrogen bonds have been suggested to have covalent character based on investigations by diverse experimental techniques including IR,⁷ X–N deformation densities,⁸ and topological analysis of experimental electron densities,^{9,10} and have been surveyed with crystal structure correlations.¹¹ To shed more light on the electronic features of short hydrogen bonds in conjugated systems, we have reinvestigated the crystal structure of benzoylacetone (1-phenyl-1,3-butadione), a representative example of an unsymmetrical *cis*-enol system with a short intramolecular O–H...O hydrogen bond, by a combined X-ray and neutron diffraction study at very low temperatures. We use the neutron data to determine the best structural model, and then determine the electron density distribution (EDD) based on combined analysis of the X-ray and neutron diffraction data. A topological analysis¹² of the EDD makes it possible to examine the nature of the bonding and provides a direct comparison with results obtained for systems lacking conjugation. In a related paper¹³ we explain in detail the elaborate crystallographic procedures and describe the behavior of a benzoylacetone crystal cooled from 300 to 8 K.

Experimental Section

The Neutron Diffraction Study. Commercially available benzoylacetone was purified by sublimation and recrystallized from pentane. Neutron diffraction data were collected at beamline TAS2 at reactor DR3 of Risø National Laboratory, Roskilde, Denmark, using a four-circle diffractometer fitted with a closed-cycle He refrigerator. Experimental details are given in Table 1.

The main purpose of the neutron diffraction study was to establish the correct low-temperature structural model, in particular with respect to the position and the thermal behavior of the enol hydrogen atom. This is impossible to do from X-ray data alone, and the exact structural model is crucial for the understanding of short hydrogen bonds. The neutron data were also used to determine the positional and the thermal parameters of all the other hydrogen atoms, and they were subsequently used as fixed values in refinements of the X-ray data. The disorder

(5) Herbstein F. H.; Kapon, M.; Reisner, G. M.; Lehmann M. S.; Kress, R. B.; Wilson R. B.; Shiau, W. I.; Duesler, E. N.; Paul, I. C.; Curtin, D. Y. *Proc. R. Soc. London* **1985**, 399, 295–319.

(6) Larsen, F. K. *Acta Crystallogr. Sect. B* **1995**, 51, 468–482.

(7) Reid, C. J. *J. Chem. Phys.* **1959**, 30, 182–190.

(8) Stevens, E. D.; Lehmann, M. S.; Coppens, P. *J. Am. Chem. Soc.* **1977**, 99, 2829–2831.

(9) Flensburg, C.; Larsen, S.; Stewart, R. F. *J. Phys. Chem.* **1995**, 99, 10130–10141.

(10) Mallinson, P. R.; Wozniak, K.; Smith, G. T.; McCormack, K. L. *J. Am. Chem. Soc.* **1997**, 119, 11502–11509.

(11) Gilli, P.; Bertolasi, V.; Ferretti, V.; Gilli, G. *J. Am. Chem. Soc.* **1994**, 116, 909–915.

(12) Bader, R. F. W. *Atoms in molecules. A quantum theory*; Oxford University Press: Oxford, 1990. Calculated at the HF/6-31* level of theory, benzene C–C bonds show $\rho_b = 2.205 \text{ e}/\text{\AA}^3$ and $\nabla^2\rho_b = -24.4 \text{ e}/\text{\AA}^5$.

(13) Herbstein, F. H.; Kapon, M.; Reisner, G. M.; Madsen, G. K. H.; Iversen, B. B.; Larsen, F. K. *Acta Crystallogr., Sect. B* **1998**, in preparation.

Table 1. Experimental Details for Benzoylacetone

	X-ray study	Neutron study
	crystal data	
chemical formula	C ₁₀ H ₁₀ O ₂	C ₁₀ H ₁₀ O ₂
chemical formula wt	162.188	162.188
space group	monoclinic <i>P</i> 2 ₁ / <i>c</i>	monoclinic <i>P</i> 2 ₁ / <i>c</i>
<i>a</i> (Å)	8.006(3)	8.027(7)
<i>b</i> (Å)	5.482(3)	5.483(2)
<i>c</i> (Å)	19.444(8)	19.478(13)
β (°)	110.46(3)	110.42(5)
<i>V</i> (Å ³)	799.5(5)	803.4(6)
<i>Z</i>	4	4
<i>D_x</i> (Mg m ⁻³)	1.350	
radiation	Ag K α	neutrons
wavelength (Å)	0.5616	1.012
temp (K)	8.4(4)	20(1)
crystal morphology	colorless spherical crystal of 0.3 mm diameter	colorless crystal bounded by [100] 1.2 mm, [010] 6.0 mm, [001] 2.8 mm
	data collection	
diffractometer	Type 512 HUBER	Type 512 HUBER
cooling	CS 202 DISPLEX	CS 201 DISPLEX
scan method	ω -2 θ	ω -2 θ
no. of measured reflcns	10494	2722
no. of unique reflcns	2862	1597
no. obsd reflcns (<i>I</i> > 2 σ (<i>I</i>))	2013	1236
internal agreement (%)	2.4	2.3
	refinement	
refinement on	<i>F</i> ²	<i>F</i> ²
<i>R</i> (<i>F</i>), <i>R</i> (<i>F</i> ²) (%)	2.56, 3.17	5.16, 6.10
<i>wR</i> (<i>F</i>), <i>wR</i> (<i>F</i> ²) (%)	2.31, 4.47	5.00, 8.40
GOF	0.900	2.250
<i>N</i> _{obs} , <i>N</i> _{par}	2013, 307	1236, 219

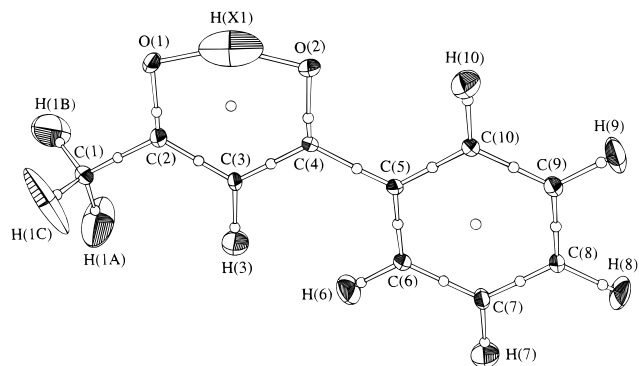


Figure 2. ORTEP drawing of the benzoylacetone molecule showing the atom numbering scheme and 50% probability ellipsoids determined by refinement of the 20K neutron data. Open circles are critical points calculated in the topological analysis

model, with two differently populated hydrogen positions between the keto and enol oxygen atoms, and the order model were both tested extensively in least-squares refinements. An ORTEP¹⁴ plot of the molecule, corresponding to the best model, the order model, is shown in Figure 2.

The reasons for favoring the order model over the disorder model are presented in detail in ref 13. Two main reasons are the following. First of all, the residual map from a refinement of the structure without an enol hydrogen showed only one large minimum between the oxygen atoms, Figure 3.

Second, Hirshfeld's rigid bond test¹⁵ applied in an analysis of the Atomic Displacement Parameters (ADP's) indicated no disorder.¹⁶ The neutron data provide direct evidence for a structural model with an

(14) Johnson, C. K. *ORTEP* program; Report ORNL-5138, Oak Ridge National Laboratory: Oak Ridge, TN 1976.

(15) Hirshfeld, F. L. *Acta Crystallogr., Sect. A* **1976**, 32, 239–244.

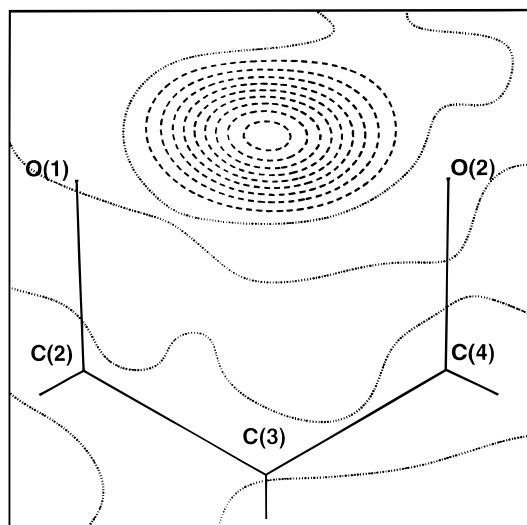


Figure 3. Difference map from the neutron refinement with the enol hydrogen atom omitted from the model. The contour interval is $0.05 \times 10^{-14} \text{ m}^3/\text{Å}^3$. Broken lines represent negative contours and solid lines positive contours. The dotted line is the zero contour. Hydrogen has a negative scattering factor, so the missing enol hydrogen appears as the negative area in the map.

Table 2. Selected Interatomic Distances and Bond Angles Determined in the Neutron Diffraction Study

		bond length, Å			
O(1)–O(2)	2.502(4)	C(2)–O(1)	1.286(4)	C(2)–C(3)	1.414(4)
O(1)–H(X1)	1.329(11)	C(4)–O(2)	1.293(4)	C(3)–C(4)	1.405(4)
O(2)–H(X1)	1.245(11)	C(1)–C(2)	1.499(4)	C(4)–C(5)	1.483(4)
		angle, deg			
O(1)–H(X1)–O(2)	152.3(6)	C(1)–C(2)–C(3)			120.9(2)
C(2)–O(1)–H(X1)	101.2(4)	C(2)–C(3)–C(4)			119.7(2)
C(4)–O(2)–H(X1)	103.2(4)	O(2)–C(4)–C(3)			120.9(3)
O(1)–C(2)–C(1)	117.0(3)	O(2)–C(4)–C(5)			116.4(3)
O(1)–C(2)–C(3)	122.1(3)	C(3)–C(4)–C(5)			122.6(2)

ordered enol hydrogen atom positioned asymmetrically between the oxygen atoms. The molecular geometry is given in Table 2. The large ADP's of the enol hydrogen can be explained if the hydrogen resides in a large, flat potential well. If the enol hydrogen sits in a very flat potential, we might expect anharmonicity in its thermal motion. To test this we have included third- and fourth-order Gram–Charlier coefficients¹⁷ on the enol hydrogen. Introduction of anharmonic parameters leads to a marginal drop in the *R* factor, but a couple of the fourth order coefficients refined to significant values at a 2σ level. None of the third-order terms were significant, so they were excluded from the final model.

The X-ray Diffraction Study. The crystal was encapsulated in a glass capillary to prevent sublimation. Data were collected on a four-circle diffractometer fitted with a closed-cycle helium refrigerator. Data collection lasted 5 weeks, and the temperature was kept constant at 8.4(4) K. Experimental details are given in Table 1. The X-ray data were fitted to the aspherical atom formalism developed by Stewart¹⁸ and Hansen and Coppens.¹⁹ The multipole refinement of the X-ray data was carried out with the program XD.²⁰ The atomic density contributions are parametrized according to the expression

$$\rho_{\text{atom}}(\mathbf{r}) = P_{\text{core}}\rho_{\text{core}} + P_{\text{valence}}\kappa^3\rho_{\text{valence}}(\kappa\mathbf{r}) + \sum_{l=0}^{l_{\text{max}}} \kappa_l^3 R_l(\kappa_l\mathbf{r}) \sum_{m=0}^l P_{lm\pm} d_{lm\pm}(\theta, \varphi)$$

In this equation R_l values are radial functions, $d_{lm\pm}$ values are angular functions, κ values are expansion/contraction coefficients, and P values are populations of the individual functions. The hydrogens were fixed at the positions found in the neutron study. Atomic displacement parameters for the hydrogen atoms were derived according to Blessing's²¹ scaling procedure applied to parameters determined from separate refinements of the X-ray and neutron data.

On the carbon and oxygen atom positions functional expansions up to octapole level were introduced, whereas the expansions were broken at quadrupole level at the hydrogen positions. All atoms were given a κ expansion/contraction parameter for the spherical monopole term. The radial dependencies of the different types of atoms were constrained to be equal. Refinements with separate κ' values for the multipoles were attempted, but this did not give satisfactory results and $\kappa' = 1$ was used in the final refinement. Chemical constraints were introduced for the benzene ring and the methyl group. For carbon and oxygen both the core and valence scattering factors were calculated from Hartree–Fock atomic wave functions,²² and for hydrogen, the scattering factors calculated by Stewart, Davidson, and Simpson²³ were used. Information on the refinement is given in Table 1. The corresponding residual density map shows no significant features and a maximum value of $0.15 \text{ e}/\text{Å}^3$. A complete list of refined electron density parameters is given as Supporting Information. Net atomic charges defined as the atomic number, Z , minus the sum of the core population, P_{core} , and the spherical valence population, P_{valence} are small and insignificant except for the atoms involved in the intramolecular hydrogen bond. O1 has a charge of $-0.45(4) \text{ e}$, O2 has $-0.51(5) \text{ e}$, and H(X1) has $0.40(3) \text{ e}$. A noticeable feature of the electron density parameters is the low monopole population, $M1 = 0.60(3)\text{e}$, of the enol hydrogen H(X1). This corroborates evidence from NMR experiments which show remarkable downfield shift of the cyclic enolic proton signal, indicating deshielded protons.²⁴

The model deformation density map, Figure 4, contains the expected charge accumulations due to bonding between the atoms. Generally, a deficiency of charge is noted at the hydrogen positions, especially so for the H(X1) hydrogen atom that is involved in the RAHB.

Discussion

Structural Properties. Selected interatomic distances and angles are given in Table 2. The Supporting Information contains a full description of the geometry as determined in both the X-ray and the neutron study. The keto–enol group is quite symmetric. The two C–O bond lengths deviate by just two standard deviations and have values midway between typical C=O ($\approx 1.20 \text{ Å}$) and C–O ($\approx 1.37 \text{ Å}$) bond lengths. Something similar can be said about the C–C bonds of the keto–enol group, which fall between the typical values of C=C ($\approx 1.33 \text{ Å}$) and C–C ($\approx 1.48 \text{ Å}$) bond lengths. The equivalence of the bond lengths may be attributed to delocalization over a conjugated π -bonded system in the keto–enol group. The hydrogen bond is short compared to a normal ionic hydrogen bond and the two O–H distances are almost equal. Structural refinements based on the neutron diffraction data

(16) For reviews on the use of ADP's for detecting disorder see: Dunitz, J. D.; Schomaker, V.; Trueblood, K. N. *J. Phys. Chem.* **1988**, *92*, 856–867. Dunitz, J. D.; Maverick, E. F.; Trueblood, K. N. *Angew. Chem., Int. Ed. Engl.* **1988**, *27*, 880–895.

(17) Johnson, C. K.; Levy, H. A. *In International Tables of X-ray Crystallography*; Kynoch Press: Birmingham, 1974; Vol. IV, pp 311–316.

(18) Stewart, R. F. *J. Chem. Phys.* **1973**, *58*, 1668–1676.

(19) Hansen, N. K.; Coppens, P. *Acta Crystallogr., Sect. A* **1978**, *34*, 904–921.

(20) Koritsanszky, T.; Howard, S. T.; Mallinson, P. R.; Su, Z.; Richter, T.; Hansen, N. K. *XD* program, a computer program package for multipole refinement and analysis of charge densities from diffraction data, 1995; Institute of Crystallography, Freie Universität, Berlin, Germany.

(21) Blessing, R. H. *Acta Crystallogr., Sect. B* **1995**, *51*, 816–823.

(22) Clementi, E.; Roetti, C. *At. Data Nucl. Data Tables* **1974**, *14*, 177–478.

(23) Stewart, R. F.; Davidson, E. R.; Simpson, K. T. *J. Chem. Phys.* **1965**, *42*, 3175–3187.

(24) Bertolasi, V.; Gilli, P.; Ferretti, V.; Gilli, G. *J. Chem. Soc., Perkin Trans. 2* **1997**, 945–952.

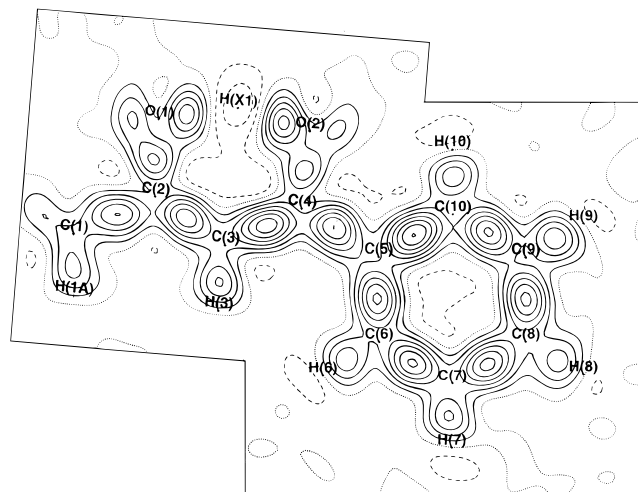


Figure 4. Model deformation density. The enol part is plotted in the plane of the enol group, and the phenyl part is plotted in the plane of the phenyl group. There is an angle of 6.4° between the two planes. The contour interval is $0.1 \text{ e}/\text{\AA}^3$. The dotted line is the zero contour. Solid lines are positive contours, broken lines negative contours.

showed that the hydrogen is positioned asymmetrically, closer to O(2) than to O(1) (see Table 2). The asymmetrical nature of the hydrogen bond fits with the other bond distances in the keto-enol group, and a model with slight conjugation. The C(2)–C(3) and C(3)–C(4) bond lengths also deviate by just two standard deviations. If the hydrogen is bonded more strongly to O(2) than to O(1) then C(4)–O(2) should have less double bond character than C(2)–O(1). Similarly C(3)–C(2) should have less double bond character than C(3)–C(4). This is exactly what the bond distances suggest, and the bond distances are in excellent agreement with the RAHB model proposed by Gilli et al.² The hydrogen is positioned closest to the oxygen that is bonded to the carbon adjacent to the more electron withdrawing group. In agreement with the RAHB model the bond lengths suggest a large degree of π -delocalization, and the O–H–O distance is very short.

Topological Analysis. The topological analysis of electron densities as developed by Bader and co-workers has been extensively presented in the literature.¹² The positions of the bond critical points (CPs) found in the static model density by the XD program are shown in Figure 2. CPs are points in the electron density where the first derivative of the electron density vanishes. The eigenvalues of the second derivatives, their sums (the Laplacian $\nabla^2\rho_b$) calculated at the bond CPs, the length of the bond paths, and the internuclear distances are listed in Table 3.

Examination of the values of ρ_b and $\nabla^2\rho_b$ in the benzene ring provides a first test of the reliability of the static model EDD. For the benzene ring the ρ_b and the $\nabla^2\rho_b$ values are in close agreement with published experimental²⁵ and theoretical¹² values. Calculation of credible bond ellipticities requires very good quality data since they are the ratio of second derivatives of ρ . As seen in Table 3 the ellipticities in the benzene ring vary from 0.21 to 0.26 for C–C bonds, which is also in very good agreement with literature values. As expected, a ring critical point is found close to the center of the benzene ring, as shown in Figure 2. The topological features of the benzene

(25) Stewart, R. F. In *The Application of Charge Density Research to Chemistry and Drug Design*; NATO-ASI Ser. B; Jeffrey, G. A., Piniella, J. F., Eds.; Plenum Press: New York, 1991; Vol. 250, pp 63–101. Based on 123K diffraction data Stewart has calculated ρ_b and $\nabla^2\rho_b$ of a benzene ring. In the C–C bonds ρ_b range from 2.12 to 2.19 $\text{e}/\text{\AA}^3$ and $\nabla^2\rho_b$ from -16.3 to $-17.6 \text{ e}/\text{\AA}^5$.

ring have an excellent internal consistency, and agree well with other studies.

The values of ρ_b and $\nabla^2\rho$ for the C–H bonds of the methyl group are similar to those of the C–H bonds of benzene. As for benzene, the small ellipticities of the C–H bonds confirm the expected picture of a single bond dominated by σ contributions. From the model of benzoylacetone one expects that C(1)–C(2) and C(4)–C(5) will be predominantly single bonds. The values of ρ_b in these bonds are identical within one standard deviation and are smaller than the ρ_b in the benzene ring. The ellipticities are both $\epsilon = 0.15$, and as expected they are smaller than the ellipticities of the benzene-ring bonds. Nevertheless, they are higher than what would be expected for normal single bonds. This is in agreement with what Bader et al.²⁶ find in theoretical calculations. The ellipticities of formal single bonds can be larger than zero, if the atoms involved are linked to an unsaturated system.

The Keto–Enol Group. Chemically the most interesting group in benzoylacetone is the keto-enol group. The ρ_b 's in the C(2)–C(3) and C(3)–C(4) bonds are 2.04(4) and 2.17(4) $\text{e}/\text{\AA}^3$, respectively, close to the values obtained for the C–C bonds in the benzene ring. The π delocalization predicted from analysis of the bond lengths is truly reflected in the topology of the static model EDD. Thus the ellipticities of the C(2)–C(3) and C(3)–C(4) bonds are close to the ellipticities in the benzene ring. The model also predicts π delocalization in the C–O bonds. As seen from Table 3, values of ellipticities do suggest the presence of a delocalized π system in the whole keto-enol group in accord with the symmetry in bond lengths. The fact that ρ_b and ϵ in the C(3)–C(4) bond are larger than ρ_b and ϵ in C(2)–C(3) supports the slightly asymmetric position of the enol hydrogen, which predicts that C(3)–C(4) has more double bond character than C(2)–C(3). A similar pattern is indicated for ρ_b in C(2)–O(1) and C(4)–O(2). The CPs in the C–O and O–H bonds lie closer to the carbons and the hydrogen than to the oxygens. This is a result of the electronegative oxygens having accumulated charge, leading to an expansion of the atomic basin of the oxygens. As expected a (3,+1) critical point is found inside the keto-enol ring, almost at the center of the carbons and the oxygens.

The critical points of the two O–H bonds do not appear in Figure 2 because they are hidden behind the extended atomic displacement ellipsoid of the H(X1) atom at distances of 1.02 and 1.00 \AA from H(X1), but they are shown in Figure 5. For both the bonds we obtain relatively large values of the density ρ_b at the bond critical point (0.76(3) and 0.89(3) $\text{e}/\text{\AA}^3$). For conventional hydrogen bonds ρ_b values of 0.05–0.23 $\text{e}/\text{\AA}^3$ have been reported.²⁷ The relatively small values for ellipticities of the O(1)–H(X1) and O(2)–H(X1) suggest that the bonding originates mainly from σ contributions. To further characterize the keto-enol ring the negative of the Laplacian distribution, which provides a mapping of local charge depletion and concentration, was calculated. A contour plot of that part of the molecule is shown as Figure 5. The lone pairs on the oxygens, as well as the bonding electron pairs, indicating shared interactions in the C–C bonds, and the C–O bonds are clearly visible. Table 3 shows these bonds have large negative values of the Laplacian at their bond critical points, as also seen from Figure 5, which shows that the negative Laplacian forms a contiguous positive area over the valence region of neighboring C and O atoms. Both O–H bonds also have negative values

(26) Bader, R. F. W.; Sleet, T. S.; Cremer, D.; Kraka, F. *J. Am. Chem. Soc.* **1983**, *105*, 5061–5068.

(27) Carroll, M. T.; Bader, R. F. W. *Mol. Phys.* **1988**, *65*, 695–722.

Table 3. Critical Points in the Static Model Density^a

bond	λ_1	λ_2	λ_3	$\rho_b, e/\text{\AA}^3$	$\nabla^2\rho_b, e/\text{\AA}^5$	ϵ	$d_{1-\text{cp}}, \text{\AA}$	$d_{2-\text{cp}}, \text{\AA}$	$R_{1-2}, \text{\AA}$
O(1)–H(X1)	–8.43	–7.63	11.53	0.76(3)	–4.5(2)	0.10	1.021	0.306	1.33
O(2)–H(X1)	–12.26	–10.64	13.78	0.89(3)	–9.1(2)	0.15	0.999	0.249	1.25
O(1)–C(2)	–23.03	–20.89	14.90	2.54(8)	–29.0(4)	0.10	0.788	0.497	1.29
O(2)–C(4)	–22.24	–18.34	14.56	2.44(8)	–26.0(4)	0.21	0.798	0.497	1.30
C(1)–C(2)	–13.73	–11.92	12.92	1.82(4)	–12.72(8)	0.15	0.722	0.773	1.49
C(1)–H(1A)	–17.69	–15.91	12.86	1.69(3)	–20.7(1)	0.11	0.767	0.294	1.06
C(1)–H(1B)	–17.13	–16.31	13.05	1.68(3)	–20.40(5)	0.05	0.771	0.294	1.06
C(1)–H(1C)	–17.43	–16.35	13.21	1.70(3)	–20.57(5)	0.07	0.761	0.289	1.05
C(2)–C(3)	–15.84	–12.70	12.39	2.04(4)	–16.15(9)	0.25	0.747	0.662	1.41
C(3)–C(4)	–17.88	–13.86	13.53	2.17(4)	–18.20(9)	0.29	0.675	0.727	1.40
C(3)–H(3)	–18.33	–17.70	13.21	1.72(3)	–22.8(2)	0.04	0.788	0.288	1.08
C(4)–C(5)	–13.88	–12.03	12.86	1.84(3)	–13.0(9)	0.15	0.797	0.684	1.48
C(5)–C(6)	–17.05	–14.01	13.26	2.15(4)	–17.80(8)	0.22	0.689	0.714	1.40
C(5)–C(10)	–17.62	–13.97	13.81	2.19(4)	–17.78(9)	0.26	0.704	0.701	1.40
C(6)–C(7)	–16.96	–13.98	12.64	2.15(3)	–18.31(7)	0.21	0.718	0.674	1.39
C(6)–H(6)	–18.91	–17.36	11.88	1.70(2)	–24.4(1)	0.09	0.791	0.288	1.08
C(7)–C(8)	–17.02	–13.86	13.42	2.18(4)	–17.5(9)	0.23	0.716	0.679	1.40
C(7)–H(7)	–18.32	–17.78	13.47	1.65(2)	–22.6(1)	0.03	0.818	0.270	1.09
C(8)–C(9)	–16.85	–13.79	13.37	2.17(5)	–17.3(1)	0.22	0.677	0.718	1.39
C(8)–H(8)	–17.14	–15.91	12.31	1.66(3)	–20.7(2)	0.08	0.779	0.308	1.09
C(9)–C(10)	–16.93	–13.95	12.65	2.14(3)	–18.23(7)	0.21	0.674	0.718	1.39
C(9)–H(9)	–18.03	–17.49	13.40	1.64(2)	–22.1(1)	0.03	0.820	0.272	1.09
C(10)–H(10)	–18.83	–17.27	11.84	1.69(2)	–24.3(1)	0.09	0.793	0.289	1.08
phenyl ring CP	–0.30	1.67	1.80	0.168	3.2				
enol ring CP	–0.36	1.78	2.37	0.134	3.8				
Citrinin O–H bonds ⁵⁰									O–H distance
O11–H11	–42.75	–40.72	33.68	2.33(7)	–49.8(70)	0.050			0.974
O17–H11	–3.39	–2.89	8.54	0.44(19)	2.25(6)	0.174			1.625
O18–H18	–32.76	–30.70	30.03	2.06(6)	–33.4(53)	0.067			1.056
O13–H18	–6.49	–5.40	11.99	0.65(26)	0.10(12)	0.203			1.461

^a $\lambda_1, \lambda_2,$ and λ_3 are the eigenvalues of the Hessian matrix. ρ_b is the electron density and $\nabla^2\rho_b$ is the Laplacian at the CP. ϵ is the ellipticity. $d_{1-\text{cp}}$ and $d_{2-\text{cp}}$ are the distances from the atoms to the critical point. R_{1-2} is the sum of $d_{1-\text{cp}}$ and $d_{2-\text{cp}}$.

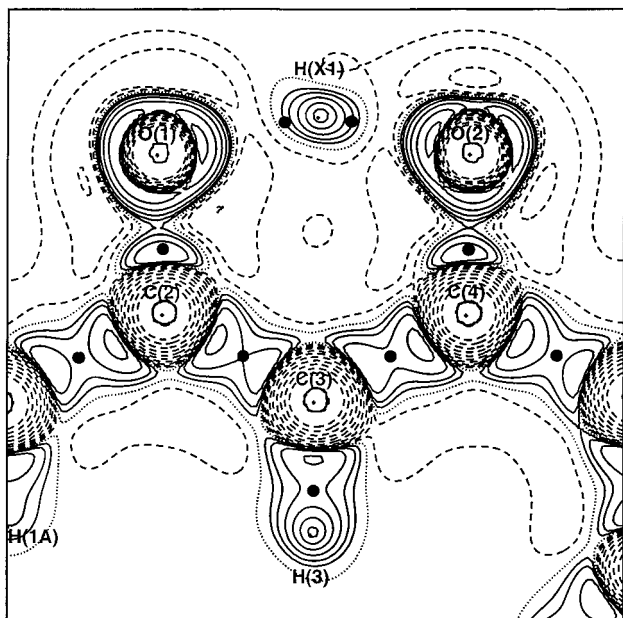


Figure 5. Contour plot of the negative of the Laplacian of the electron density in the plane of the keto–enol group. The contours are drawn at logarithmic intervals of $1.0 \times 2^N e \text{\AA}^{-5}$. The dotted line is the zero contour. Solid lines are positive contours, broken lines negative contours. The first two positive and negative contours are omitted for clarity. Bond critical points are marked with solid in circles.

of the Laplacian at their bond critical points, the usual characteristic of shared interactions. However, Figure 5 shows that the negative Laplacian has a slightly negative area surrounding completely the keto–enol hydrogen atom, which means that the Valence Shell Charge Concentrations (VSCCs) of the two oxygen atoms are very well separated from the VSCC

of the hydrogen atom. This would be expected for nonshared interactions. The occurrence of negative Laplacian at the bond critical point is likely to be due to the short bond length of these nonshared interactions, which causes the minimum of the density along the bond path to fall within the VSCC of the hydrogen atom. On the other hand, the pronounced polarization at both oxygens of the lone pair facing the hydrogen atom and of the VSCC of the latter shows that the O–H interactions are far from being purely ionic in nature. The topology of the electron density was also used to decide whether intermolecular hydrogen bonds are present. The EDD between the enol hydrogen and the oxygens in a neighboring molecule was searched for CPs, but none were found.

Gilli et al.² compiled a list of *cis*-enol compounds which showed that a high degree of symmetry of the keto–enol group correlates with a short O–H···O hydrogen bond and a lengthening of the O–H bond. The concept of resonance assisted hydrogen bonding was developed. Excluded from the list were molecules with fragments carrying other heteroatoms than oxygen or participating in aromatic rings. Thus, a short O–H···O hydrogen bond is not equivalent with a symmetric keto–enol ring and the electronic nature of the hydrogen bond cannot be inferred solely from the distance between oxygen atoms of the hydrogen bond. This is evident when comparing our results with those of the detailed low-temperature (19 K) X-ray diffraction charge density study of crystalline citrinin²⁸ which has an aromatic ring and attached to it two keto–enol like ring systems with 2.5 Å intramolecular O–H···O hydrogen bonds. The bond lengths and the topology within the keto–enol rings are quite different relative to those of benzoylacetone, see Table 3. The two fused ring systems of citrinin have

(28) Roversi, P.; Barzaghi, M.; Merati, F.; Destro, R. *Can. J. Chem.* **1996**, *74*, 1145–1161.

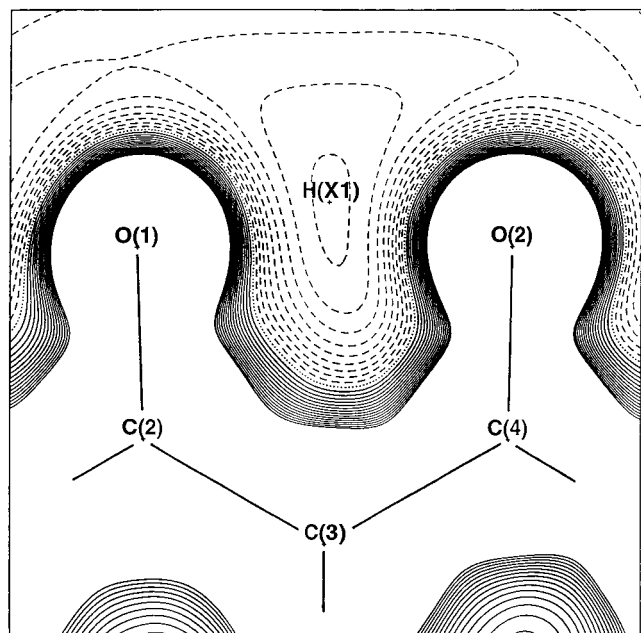


Figure 6. Close up of the electrostatic potential in the enol region calculated after removal of the contribution of the enol hydrogen. The contour interval is $0.05 \text{ e}/\text{\AA}$. The cutoff is at $0.75 \text{ e}/\text{\AA}$.

distinctly alternating bond lengths in contrast to benzoylacetone. Also the hydrogen atoms in the $\text{O}-\text{H}\cdots\text{O}$ bonds of citrinin sit much more asymmetrically, closely bound to the enol oxygen atom. Moreover, properties of ρ at the bond critical points of the intramolecular hydrogen bonds in citrinin each show one strongly negative Laplacian and one positive. Correspondingly, it must be concluded that the hydrogen atoms in the citrinin intramolecular hydrogen bonds are covalently bonded on one side and more weakly electrostatically bonded to the other side. This is in contrast to benzoylacetone where hydrogen has covalent and electrostatic bonding contributions to both oxygen atoms in the resonance assisted intramolecular hydrogen bond.

Electrostatic Potential. The multipole model reveals that there are large formal charges on the oxygens and the enol hydrogen in benzoylacetone, and the CPs in the hydrogen bond sit much closer to the hydrogen than to the oxygens. This suggests polar bonds and thus an electrostatic contribution to the stabilization of the enol hydrogen. To investigate this aspect, the electrostatic potential has been calculated by the method of Su and Coppens²⁹ which is based on the populations of the multipoles found in the refinement. In Figure 6 is shown a closeup of the keto-enol part of the molecule of the electrostatic potential calculated after removal of the contribution of the enol hydrogen. The enol hydrogen sits in a large flat-bottomed electrostatic potential shaped as a trench perpendicular to the line connecting the oxygen atoms. On the basis of the shape of the electrostatic potential alone one would expect a large vibrational amplitude of the hydrogen perpendicular to the line connecting the two oxygen atoms. The fact that this is not observed conforms with the topological analysis that indicated covalent contributions to the $\text{O}-\text{H}$ bonding.

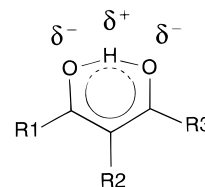


Figure 7. The modified resonance assisted hydrogen bonding model.

RAHB Model. The substantial formal charges on the hydrogen and the oxygens, determined by the multipole analysis, may be included in the RAHB model to give a more adequate description of the partly covalent and partly electrostatic bonding. We have therefore modified the RAHB model of benzoylacetone slightly to the one shown in Figure 7. The charges in the keto-enol ring can be explained in terms of RAHB. If the resonance induces charges as shown in Figure 7, RAHB can compensate, not only by moving the hydrogen toward the keto oxygen atom but also by moving negative charge from the hydrogen onto the original enol oxygen atom. In this model, RAHB can be described as a feedback mechanism that drives the charges in the ring toward symmetry.

Conclusion

In our study of benzoylacetone we have found no evidence of disorder in the keto-enol group. The diffraction data provide support for location of the enol hydrogen in a very flat asymmetric single minimum potential. The EDD derived from combined analysis of the neutron and X-ray diffraction data shows a large π -delocalization in the keto-enol group. Topological analysis of the electron density has been used to quantify the ideas about π -delocalization and to give direct evidence of the character of the intramolecular keto-enol hydrogen bond. We have found high formal charges on both the oxygens and the enol hydrogen, reflecting the fact that the hydrogen is closely bound to two electronegative atoms. It has been concluded that the bonding of the hydrogen for this short intramolecular hydrogen bond at each side of the hydrogen has partly covalent and partly electrostatic contributions. The charge density analysis led to further development of the RAHB model for resonance assisted hydrogen bonding.

Acknowledgment. Principal financial support for the project at Technion came from the U.S.-Israel Binational Science Foundation, while the Israel-Denmark Scientific Exchange Program helped to make Dr Reisner's participation in the Aarhus measurements possible. The Carlsberg Foundation is acknowledged for the low-temperature X-ray diffractometer. G.K.H.M. thanks Aarhus University for financial support. We are grateful to many colleagues for helpful discussions.

Supporting Information Available: Tables of positional parameters and displacement parameters for the neutron and the X-ray study, matrix of $\Delta_{A,B}$ values for the neutron and the X-ray study, local axes definitions, expansion/contraction κ parameters, multipole population coefficients, anharmonic displacement parameters, interatomic distances and angles, and residual density map with $0.05 \text{ e}/\text{\AA}^3$ contours (10 pages, print/PDF). See any current masthead page for ordering information and Web access instructions.

(29) Su, Z.; Coppens, P. *Acta Crystallogr., Sect. A* **1992**, *48*, 188-197.